Linear Rheology of Guar Gum Solutions

Roland H. W. Wientjes,* Michel H. G. Duits, Rob J. J. Jongschaap, and Jorrit Mellema

Rheology Group, Department of Applied Physics, University of Twente, (member Twente Institute of Mechanics and J. M. Burgers Centre), P.O. Box 217, 7500 AE Enschede, The Netherlands

Received June 20, 2000; Revised Manuscript Received October 17, 2000

ABSTRACT: We have investigated the linear viscoelastic behavior of guar gum solutions as a function of frequency, temperature, polymer concentration, and molecular weight. This was done to sort out the importance of different relaxation mechanisms like reptation or the breakup of physical bonds. In the kilohertz regime, Rouse behavior is observed. At lower frequencies, two storage modulus plateau zones were found, indicating two additional relaxations. One is operative between 1 and 100 Hz and gives rise to a very broad relaxation spectrum, even for monodisperse guar. Describing the dependencies of the relaxation time and low-shear viscosity on concentration and molecular weight with power laws resulted in unusually high coefficients. The second relaxation becomes manifest below 0.01 Hz and has not been earlier reported. Here the temperature dependence is very strong whereas all other dependencies are weak. Analyzing the experiments with existing models for transient polymer networks revealed that at best a partial decription of the experimental dependencies can be obtained. It was concluded that at least two different relaxation mechanisms must play a role, classical reptation not being one of these. Best overall predictions were obtained with a model assuming two types of associations. However, also the picture of star polymer-like structures held together via bonds with a long lifetime could give comparable predictions. For a further distinction between these mechanisms, more information about the mesoscopic structure is needed.

1. Introduction

Galactomannans are water-soluble polysaccharides found in the seed endosperm of a variety of legumes. They consist of a (1→4)-linked *β*-D-mannopyranosyl backbone partially substituted at O-6 with α-D-galactopyranosyl side groups.[6] One galactomannan which is widely used as an industrial hydrocolloid is guar gum which has a mannose:galactose ratio of 1.55. In connection to its use as a thickener in food products, several research groups have investigated the rheology of guar gum solutions.[8,9,23,26,27]

In a rheological study performed by Ross-Murphy,[28] where start shear behavior and the validity of the Cox−Merz rule were investigated, it was concluded that guar gum solutions behave like an entangled solution, as described by Doi and Edwards.[7] This conclusion was drawn despite earlier observations of Richardson and Ross-Murphy[26] who noted the onset of a transition at low shear rates (0.01 s^{-1}), although the Newtonian low-shear plateau had already been reached. Robinson et al.[27] mentioned a strong nonlinear dependence of the specific viscosity upon concentration. From this it was concluded that not only purely topological entanglements, but also specific attractive polymer−polymer interactions must play a role. Indications for this were also obtained by Goycoolea et al.[15] and by Gidley et al.,[13] who attributed a crucial role to the α-D-galactose side groups in the process of network cross-linking by semi helix−helix aggregation.

From this short overview, it is clear that the rheological behavior of guar gum solutions is still incompletely understood and that specific polymer−polymer interactions might play a role in the observed rheological behavior as well as reptation phenomena. To sort out the importance of different relaxation mechanisms, we have systematically investigated the linear viscoelastic behavior as a function of frequency, concentration, temperature, and molecular weight. To support interpretation we have characterized the molecular properties by using GPC, intrinsic viscosity measurements, and several microscopy techniques. In this paper, we will compare the linear viscoelastic behavior with predictions from existing microrheological models that take into account topological constraints and/or physical bonds.

The paper is further organized as follows. In section 2, the preparation of the solutions, the microscopic characterizations and the rheological measurement techniques are discussed. In section 3, the experimental results are shown. These results will be compared to rheological models in section 4, followed by a discussion in section 5, after which conclusions will be drawn in section 6.

2. Experimental Section

2.1. Materials. Guar gum (Meyhall) was purified from a commercial flour using a modification of the method of McCleary et al.[4] Crude guar gum (10 g) was treated with 200 mL of boiling, aqueous 80% ethanol for 10 min. The obtained slurry was collected on a glass filter (no. 3) and washed successively with ethanol, acetone, and ether. This material was added to 1 L of demiwater and allowed 1 h to hydrate. It was then stirred with a food blender (125 W), homogenized (1 min), and centrifuged at 2300*g* for 15 min. The supernatant was precipitated in two volumes of cold acetone. After redissolving in hot water, the polymer solution was ultracentrifuged at 82000*g* for 1.5 h at room temperature. The supernatant was precipitated with two volumes of ethanol. The precipitate was collected on a glass filter (no. 4) and washed with ethanol, acetone, and ether before freeze-drying. This lead to almost monodisperse purified guar gum. Only one batch of guar was purified in this laborious way, to get a monodisperse system. Solutions of this material were prepared by adding known weights of the dry guar to twice distilled water, and allowing it to hydrate for extended periods (several days) to ensure that the sample had completely dissolved. This was done at a

10.1021/ma001065p CCC: $19.00
Published on Web 12/01/2000

Table 1. Molecular Weights for Samples Prepared via Procedures I and II

guar	M_w (kD)	M_w/M_n
HM	1048	1.02
150	1400	1.1
90	1000	1.5
30	350	1.7

temperature of 277 K for concentrations between 0.4 and 2.0% (w/w). We will refer to this purification and dissolving method as procedure I.

For the purpose of characterization with Mark Houwink plots, three guar gums with different molecular weights (Meyhall) were purified with a less laborious but otherwise similar procedure. Here crude guar gum (10.0 g) was suspended in 1 L of demiwater and stirred with a food blender (125 W) for 1 min. The obtained solution was placed in a refrigerator for 24 h and then centrifuged at 22000*g* for 5 h. Then, 800 mL of the obtained supernatant was precipitated in two volumes of cold acetone. The precipitate was collected on a glass filter (no. 4) and washed with ethanol, acetone, and ether. The so obtained purified guar gum was freeze-dried and dissolved as described in procedure I. This procedure is called procedure II.

Using these procedures led to very long dissolving times. To shorten this, a third purification and dissolving procedure was used. In this procedure four different guar gums (Meyhall) with different molecular weights were purified by adding 10.0 g to 400 g acetate buffer of pH 4.66 (Merck). The slurry was homogenized for 75 s with a food blender (500 W) and centrifuged at 22000*g* for 5 h at room temperature. The supernatant (typical concentration 2% w/w) was used as a stock solution from which lower concentrations were obtained via dilution. This is procedure III. Several control experiments revealed that the rheological behavior was not significantly changed on switching from procedure II to III.

2.2. Molecular Characterization. The molecular weights of the purified guar gums using procedure I and II were determined by GPC-MALLS−RI (multiangle laser light scattering). The guar was dissolved in a 50 mM phosphate buffer with pH 8.0 to a concentration of 0.1% (w/w) and filtered through a 0.45 μm filter prior to injection. At the exit of the GPC column the (instantaneous) values of M and R_g were detected on line. The results are summarized in Table 1.

The mannose/galactose ratio of guar HM/150/90/30 was determined by HPLC after hydrolysis of the polymer to be 1.59 ± 0.05.

Molecular weights of the guar gums, obtained via procedure II, were obtained from intrinsic viscosity measurements. These experiments were done with an Ubbelohde capillary viscometer (Scott, type 532 01/0A).

From the reduced viscosity measurements, intrinsic viscosities were obtained using the Huggins equation:

$$\eta_{red} = \frac{\frac{\eta}{\eta_s} - 1}{c} = [\eta] + h_c[\eta]^2 c \qquad (1)$$

Here c is the concentration guar gum, η_{red} is the reduced viscosity, η_s is the solvent viscosity and $[\eta]$ is the intrinsic viscosity. h_c is the so-called Huggins coefficient which is a polymer constant which usually lies in the range 0.5−0.8. The Huggins coefficient was determined for all the curves and turned out to be constant within the experimental error range: 0.55 ± 0.05, which is within the expected range. With the obtained intrinsic viscosities we made a Mark−Houwink plot (Figure 2) and found the Mark−Houwink constants k_{MH} and α to be (6.7 ± 1.1) $\times 10^{-7}$ L/g and 1.05 ± 0.01. This relation was used later as a calibration curve to determine the molecular weights from intrinsic viscosity measurements for the samples made by purification procedure III.

The critical concentration where overlap between polymer chains starts to occur (c^*) and the intrinsic viscosities for the, via preparation procedure III obtained samples, were obtained

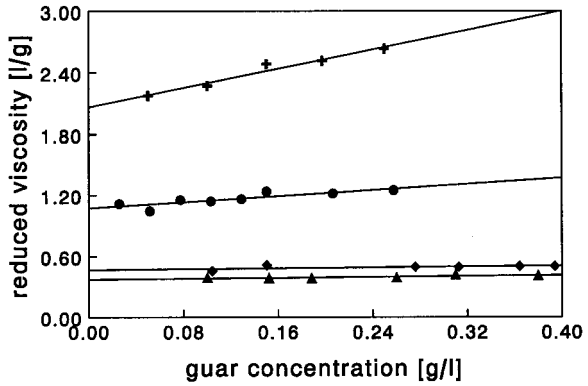

Figure 1. Reduced viscosity measurements: (▲) guar 30; (◆) guar 30 duplo; (●) guar 90; (+) guar 150.

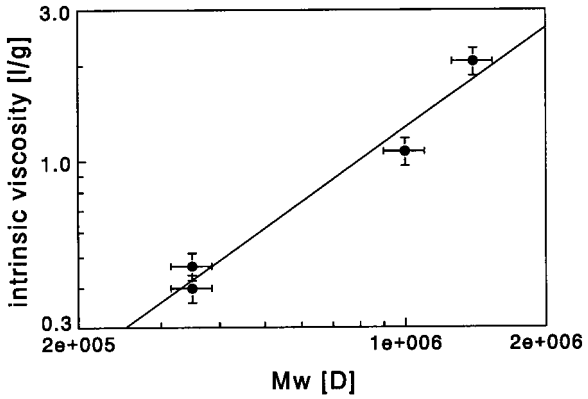

Figure 2. Mark−Houwink plot.

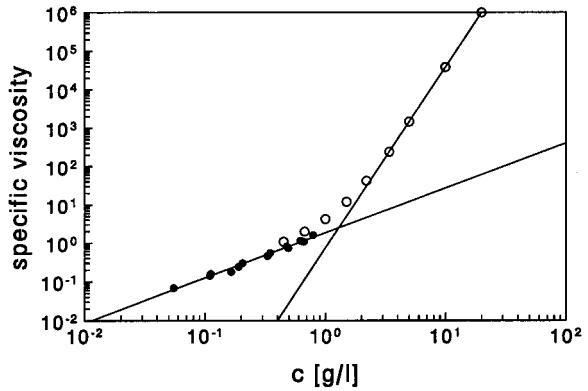

Figure 3. Determination of c^* of guar 150: (●) Ubbelohde measurements; (○) Contraves Low Shear 40 measurements.

Table 2. $[\eta]$, M_w and c^* for the Samples Prepared via Procedure III

guar	$[\eta]$ (L/g)	M_w (kD)	c^*(g/L)
150	1.217	910	1.3
90	0.958	730	2.8
60	0.510	400	4.5
30	0.333	270	4.5

from specific viscosity measurements $((\eta/\eta_s) - 1)$ as a function of concentration. Figure 3 shows a typical result. From these results we determined $c^*[\eta]$ to lie around 2 which is comparable to earlier findings of others.[19]

In Table 2, the measured intrinsic viscosities, calculated molecular weights, and critical concentrations are listed.

All measurements other than characterizations were performed at concentrations higher than c^*. Typically, three concentrations were investigated for each guar system, with the upper limit set by the extent to which the sample was sufficiently fluidlike to be manipulated.

2.3. Mesoscopic Observations. To obtain information about the mesoscopic structure of the guar gums we used three microscope methods. AFM and replica-TEM did not provide information from the bulk structure since surface and pretreatment effects were involved.

To obtain more direct information about the mesoscopic structure as present in solution, we labeled guar gum with rhodamine isothiocyanate (RITC)[1,14] and observed the solution with a Confocal scanning laser microscope via detection of the fluorescence of RITC. Since no inhomogeneities could be observed within the resolution of the instrument, it can be concluded that the guar gum solutions must be homogeneous at least down to length scales of 1 μm.

We also attempted NMR to detect hydrogen bridges and DSC to locate a possible phase transition, but without providing conclusive evidence. Also light-scattering experiments gave no useful information, since the solutions were too turbid.

2.4. Macroscopic Rheological Measurements. Linear viscoelastic moduli measurements between 10^{-3} and 2×10^{1} Hz and as a function of the temperature were performed using a Bohlin VOR with a cone and plate geometry (cone angle of 1° and 60 mm plate diameter). Measurements were conducted at six temperatures ranging from 10 to 60 °C. To avoid effects of solvent evaporation, a homemade vapor lock filled with paraffin oil was used. A correction was made for the temperature dependence of the gap width (-1.9 μm/°C) between cone and plate. To exclude inaccurate measurements, we checked the Bohlin VOR with two Newtonian fluids: water and a Baysilon oil (Bayer) with a viscosity of 300 mPa s. These testsamples showed correct results, including the limiting behavior of G' and G'' for low frequencies. Further on, we ensured that all measurements resulted in data that were clearly in the range of the torque resolution (2.35×10^{-5} N m). A 10 mL syringe was used to insert the sample. After insertion the sample was presheared at 80 s^{-1} for 1 min to obtain a homogeneously filled gap and to define the mechanical history of the sample. Then the sample was allowed to relax for 30 min before the measurements were started.

Linear viscoelastic measurements were also performed at high frequencies, using three torsion resonators and a nickel tube resonator. Those instruments were developed in our laboratory and details on design and principle can be found in Oosterbroek et al.,[24] Blom and Mellema,[2] and van den Ende et al.[10] With those instruments, dynamic moduli of weak gels can be measured at a discrete set of frequencies between 70 Hz and 250 kHz, at ambient temperatures. To allow interpretation of the results the surface loading criterion should be satisfied.[10] This means that the shear wave generated by the torsion bar must be damped significantly before it is reflected by the walls of the container. For the data presented in this paper, this criterion was satisfied.

Measurements of the viscosity as a function of shear rate were performed at 10 °C, using a Contraves Low Shear 40. A Couette geometry was used, with inner and outer radii of respectively 5.5 and 6.0 mm.

3. Results

Our rheological measurements were done with the focus to distinguish between different possible relaxation mechanisms via comparison of the results with predictions from microrheological models. To obtain an overview, we started the investigation by measuring the frequency dependence over an extended range. The results showed two storage modulus plateau zones with different temperature dependencies. These plateaus were investigated further as a function of the polymer concentration and the molecular weight.

3.1. Frequency Behavior. To map out the frequency domain we first measured the frequency dependence of a 0.4 (w/w) % monodisperse guar HM solution. For this system it was possible to cover 8 decades in frequency by using the Bohlin VOR, the torsion resonators and the nickel tube resonator. As shown in Figure 4 the data obtained from the different instruments connect well to a smooth curve.

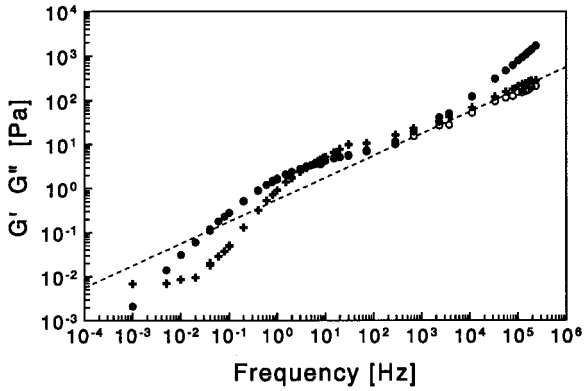

Figure 4. Linear viscoelastic behavior of a monodisperse 0.4% (w/w) guar HM solution, measured at 25 °C over an extended frequency range. The dashed line corresponds to Rouse behavior: (+) G'; (●) G''; (○) G''_{guar}.

We corrected $G''(\omega)$ for the contribution of the solvent, to allow for analysis of the loss modulus of the guar only: G''_{guar}. This correction was significant for frequencies above 10^4 Hz. The $G'(\omega)$ and the corrected $G''(\omega)$ data shown in Figure 4 make it clear that, at high frequencies, the agreement with the frequency scaling of the Rouse model[29] is very good. Both moduli follow a slope of 0.5 in the log−log plot. At frequencies below 10^3 Hz, two plateau zones for the storage modulus can be observed (at 10^{-2} and 10^1 Hz). To the best of our knowledge, this is the first time a storage modulus plateau for guar gum solutions at very low frequencies is reported.

3.2. Scaling with Temperature. For the temperature range studied, it turned out that all investigated samples showed a very similar frequency dependence above 0.03 Hz. Therefore, it was possible to obtain temperature master curves by scaling the moduli curves, measured at different temperatures, along the frequency axis. Figure 5 shows an example of the obtained master curves for $G'(\omega)$ and $G''(\omega)$. In particular, from these reduced plots, it becomes evident that at low frequencies, the storage moduli show a different temperature dependence. A plateau is observed for $G'(\omega)$, with a magnitude that increases strongly with temperature. Remarkably enough, the loss modulus $G''(\omega)$ does not show these deviations in the scaling behavior with temperature. Its slope in the log−log plot amounts to 0.8, which is close to the limiting behavior. Thus, it corroborates that only the onset of the low-frequency relaxation is observed, and that the characteristic frequency must correspond to very long time scales ($>10^3$ s). A salient detail of the relaxation spectrum within the Hz range is that it is rather broad. This wide range of relaxation times cannot be caused by polydispersity, since guar HM was almost monodisperse (see Table 1).

From the obtained frequency scaling (for frequencies above 0.03 Hz.) an Arrhenius plot was made, i.e., according to

$$a_T = \exp\left(\frac{E_{ap}}{k}\left[\frac{1}{T} - \frac{1}{T_{ref}}\right]\right) \qquad (2)$$

Here a_T is the frequency multiplication factor needed to shift the moduli curves measured at temperature T

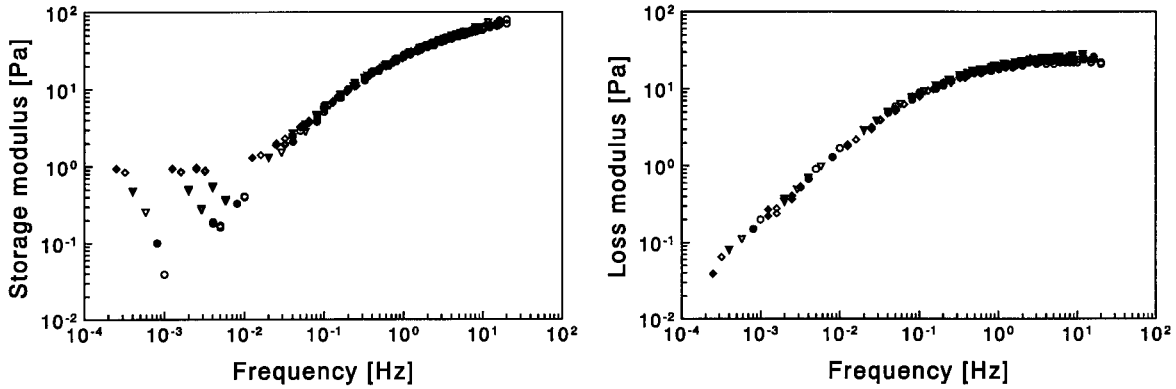

Figure 5. Moduli master curves for a 1.0% monodisperse guar HM solution (procedure I). Temperatures in °C: (◆) 60; (◊) 50; (▼) 40; (▽) 30; (●) 20; (○) 10.

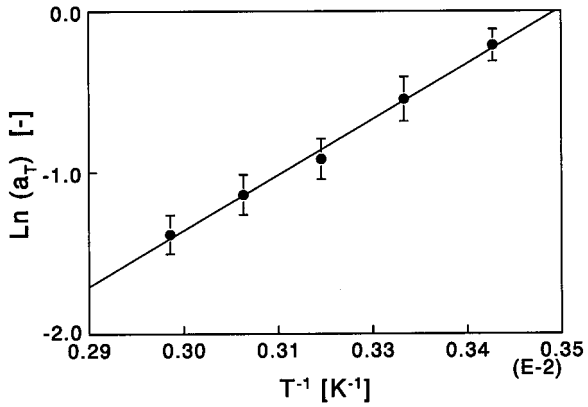

Figure 6. Arrhenius plot of the 1% (w/w) monodisperse guar HM sample.

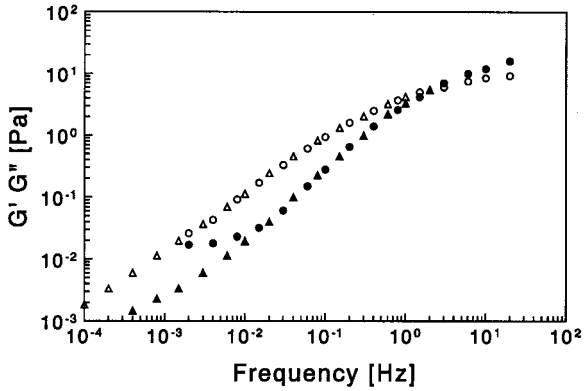

Figure 7. Master curves of 4% (w/w) guar 30 (▲, △) and 0.5% (w/w) guar 150 (●, ○) solutions: (▲, ●) storage moduli; (○, △) loss moduli.

to the modulicurves at temperature T_{ref}. E_{ap} is the apparent activation energy whereas k is the Boltzmann constant. Figure 6 shows a typical result.

From the slope, the apparent activation energy was obtained to be 10.0 ± 0.5 kT (at T = 283 K). It turned out that this apparent activation energy does not depend on the molecular weight or the guar gum concentration. Within the experimental error range, always (for all guars listed in Tables 1 and 2 and all investigated concentrations) the same apparent activation energy was obtained.

3.3. Scaling with Concentration and Molar Mass. To investigate the rheological behavior further so that comparison with microrheological models becomes possible, we studied the moduli and flow curves as a function of concentration and molecular weight. It turned out that the shape of the moduli curves at frequencies above 0.03 Hz was independent of both. To illustrate this we scaled a 4% guar 30 solution on top of a 0.5% guar 150 solution in Figure 7.

Because of this independence, all points within a curve (except for frequencies below 0.03 Hz) can be scaled onto a master curve. This makes it possible to extrapolate some curves to high frequencies. Especially interesting is that it also allows for an analysis of the concentration and molar mass dependence by considering just the scale factors. The point where $G'(\omega)$ crosses $G''(\omega)$ is very suitable for both the scaling itself and for the analysis. The inverse of the crossover frequency can be seen as a characteristic time (denoted as $\tau_{G'=G''}$). The magnitude of $G'(\omega)$ at this point (denoted as $G_{G'=G''}$) can be seen as a representation of the characteristic strength of the relaxation(spectrum). It is proportional to the high-frequency storage modulus in the absence of Rouse relaxations. The scaling results for $\tau_{G'=G''}$, and the relaxation strength as a function of concentration and molar mass are shown in Figures 8 and 9.

Also the flow curves were measured as a function of concentration and molecular weight. An example of the flow curves of guar 150 is shown in Figure 10.

The zero shear viscosities $\eta(\dot{\gamma} \rightarrow 0)$ obtained from the flow curves were found to correspond well to the low-frequency limits of $\eta'(\omega \rightarrow 0)$ estimated from $G''(\omega)$ curves (Figure 10). Such a correspondence is expected for materials that show liquidlike behavior at long time scales. It is also interesting to investigate the applicability of the Cox−Merz rule.[5] This empirical rule, stating that

$$|\eta^*(\omega)| = \sqrt{\left(\frac{G'}{\omega}\right)^2 + \left(\frac{G''}{\omega}\right)^2} = \eta(\dot{\gamma}) \quad \text{for } \omega = \dot{\gamma} \qquad (3)$$

does not apply to our guar solutions. We found that $|\eta^*(\omega)| \geq \eta(\dot{\gamma})$ for $\omega = \dot{\gamma}$, which obviously is due to the contribution of $G'(\omega)$ since $G''(\omega) \approx \eta(\dot{\gamma})\,\omega$ as mentioned before.

The power law scaling of the zero shear viscosity with the guar gum concentration and the molecular weight is shown in Figure 11. In Table 3 an overview of the measured scaling relations is given.

3.4. Low-Frequency Behavior. One of the most astonishing observations we have already presented is the storage modulus plateau at low frequencies. Although differences from the limiting linear viscoelastic behavior were observed earlier by Richardson and Ross-Murphy,[26] a second storage modulus plateau at low

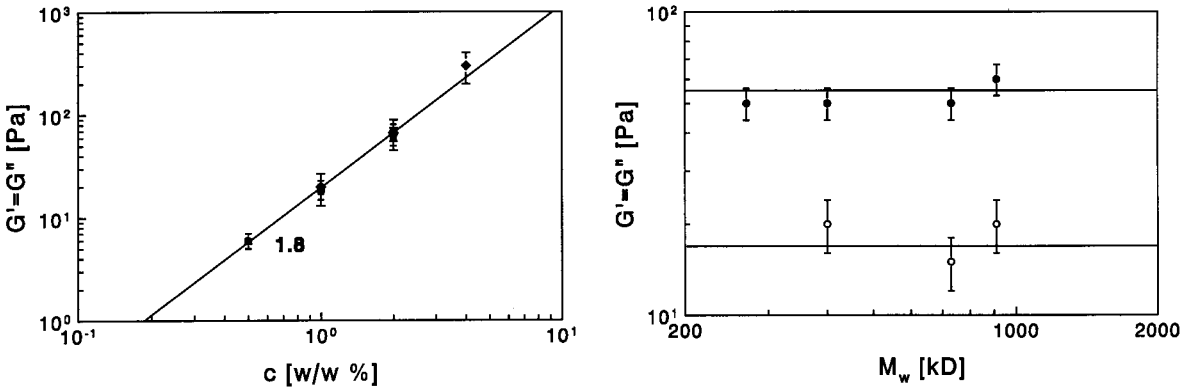

Figure 8. Storage modulus plateau vs guar gum concentration (left) and molecular weight (right). Numbers indicate power law coefficients. Left: (●) guar 150; (▲) guar 90; (▼) guar 60; (◆) guar 30. Right: (●) 2% (w/w); (○) 1% (w/w).

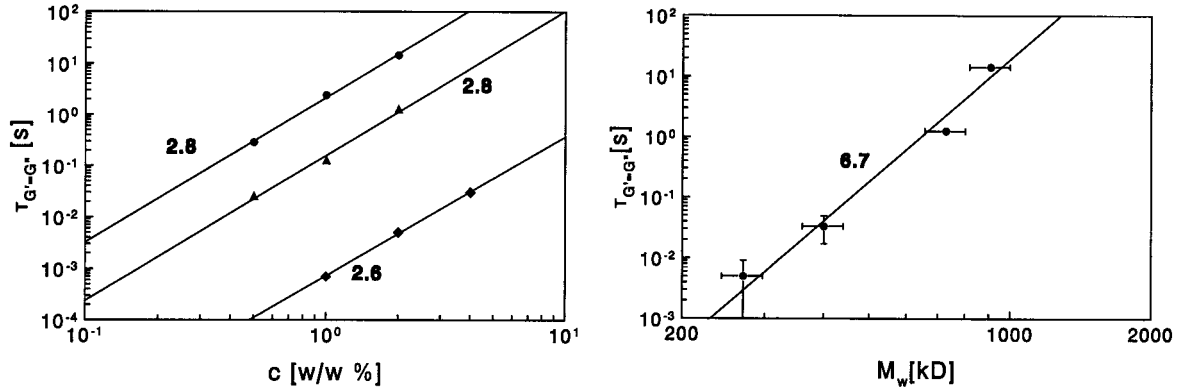

Figure 9. $\tau_{G'=G''}$ vs guar gum concentration (left) and molecular weight (right). Numbers indicate power law coefficients. Left: (●) guar 150; (▲) guar 90; (▼) guar 60; (◆) guar 30. Right: (●) 2% (w/w).

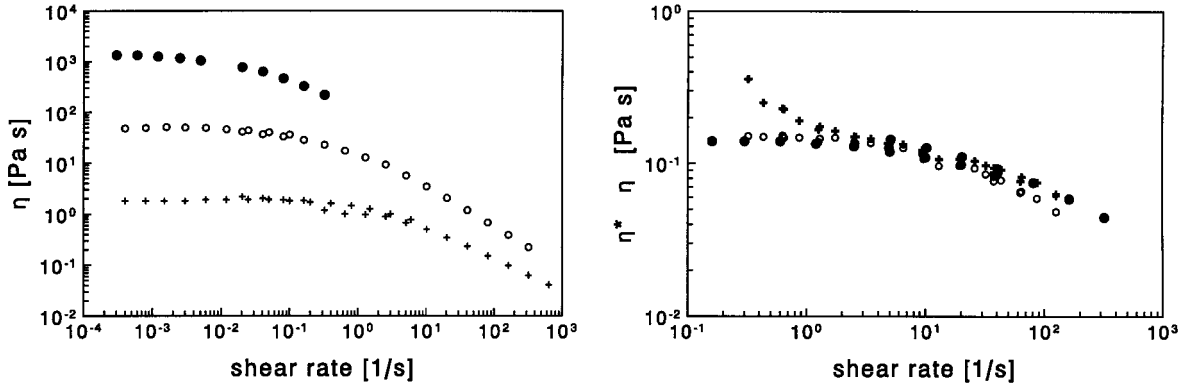

Figure 10. Left. Flow curves for guar 150 at 10 °C measured with the Contraves LS 40 (low shear rates) and the Bohlin VOR (high shear rates): (●) 2.0% (w/w); (○) 1.0% (w/w); (+) 0.5% (w/w). Right. Cox−Merz rule: (●) $\eta(\dot{\gamma})$; (○) η'; (+) η^*.

frequencies has not been reported before. It can be seen from Figure 5a that the temperature dependence of this plateau zone is rather strong. Further investigations show that there is no clear dependence on concentration and molecular weight as can be seen in Table 4.

From these data, we can conclude that there is only a very weak concentration dependence with a scaling power of 0.5 or less. Also, we can observe some correlation with molecular weight, but this dependence is not too clear.

4. Comparison with Microrheological Models

For the first time a low-frequency plateau in G' has been observed. We have observed it for differently prepared samples (including a different purification), and at different concentrations. The clear temperature dependence of this G' plateau demonstrates that the associated stress relaxation is one of a dynamic structure and not that of, e.g., a permanent rubberlike structure. In this context, we also like to note that the magnitude of the elasticity is small and that a slight shearing of the fluid is sufficient to make the plateau disappear for 15 min. Analogous behavior was found in other associating ionomers.[35] This also indicates that this behavior is of structural origin.

We have attempted to interpret the variety of observations discussed in the previous section, in the sense of identifying relaxation processes and proposing corresponding mesoscopic structure(s). Obviously a wealth of information on the structure and relaxations is contained in the measured rheological data themselves. But the problem is how to disclose it.

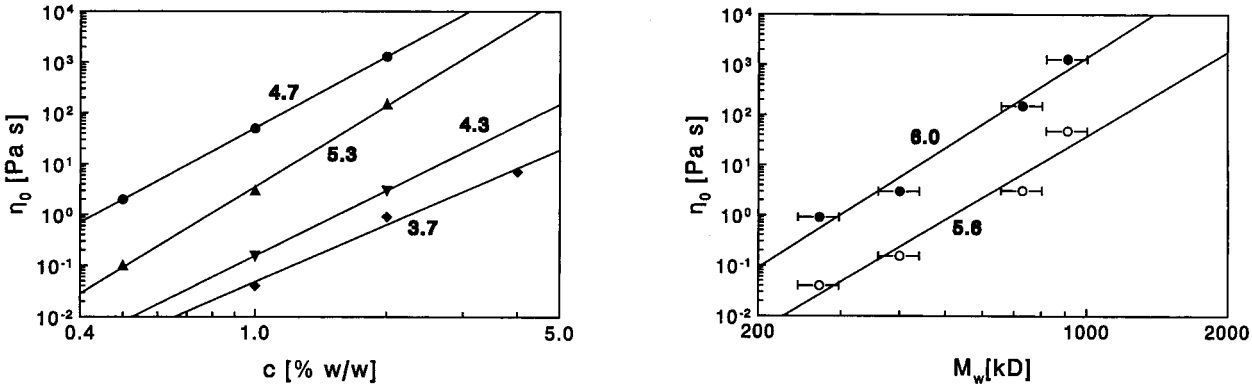

Figure 11. Zero shear viscosity zero shear viscosity vs guar concentration (left) and molecular weight (right). Numbers indicate power law coefficients. Left: (●) guar 150; (▲) guar 90; (▼) guar 60; (◆) guar 30. Right: (●) 2% (w/w); (○) 1% (w/w).

Table 3. Power Law Scaling of Linear Rheological Quantities[a]

scaling	M_w	c
η_0	5.8 ± 0.2	4.5 ± 0.8
$G_{G'=G''}$	0	1.8 ± 0.1
$\tau_{G'=G''}$	6.7 ± 0.8	2.7 ± 0.2

[a] Uncertainty ranges include differences between guar batches.

Table 4. Storage Modulus Plateau at Low Frequencies, Where lmv = Lowest Measured G' Value

guar	solvent	M_w (kD)	c (w/w%)	$G_{\text{low plateau}}$ (Pa)
HM	bidest water	1048	2.0	lmv = 1
HM	bidest water	1048	1.0	0.5
HM	bidest water	1048	0.5	0.5
150	acetate buffer	910	2.0	lmv = 0.8
150	acetate buffer	910	1.0	0.20
150	acetate buffer[a]	910	0.5	0.15
90	acetate buffer[a]	730	2.0	lmv = 0.1
90	acetate buffer[a]	730	1.0	0.20
90	acetate buffer[a]	730	0.5	0.15
30	acetate buffer[a]	270	4.0	0.02
30r	acetate buffer[a]	270	4.0	0.02
30	acetate buffer[a]	270	2.0	0.08
30r	acetate buffer[a]	270	2.0	0.04
30	acetate buffer[a]	270	1.0	lmv = 0.005
30r	acetate buffer[a]	270	1.0	lmv = 0.005

[a] Acetate buffer was used to allow comparison with a future study. The buffer did not show any other influence than to optimize the performance of an enzyme to be added.

Our first approach has been to obtain a focus for this, based on physical characterizations of the polymer structure at the mesoscopic level. Several microscopy techniques (CSLM, replica-TEM, and AFM) were applied, but no conclusive evidence about the structure at mesoscopic length scales could be obtained, other than that the guar solutions appeared to be homogeneous down to micrometer length scales (see section 2.3).

Characterizations of the chemistry of the polymer in solution can also be used to guide interpretation. Guar gum is a galactomannan chain with free mannose backbone parts. Combining this with the empirical relation between solubility and the galactose/mannose ratio of galactomannans, it is implied that the free mannose backbone parts have the tendency to form bonds when dissolved into water. Another characteristic is that all our samples were prepared above the critical overlap concentration.

Using this information we have analyzed our rheological measurements by comparing them to predictions of existing models in polymer rheology. In this comparison, we have considered the dependencies on temperature and concentration as well as molar mass, to allow for a maximum distinction between the predictions according to different models. We realize that the scope of such a comparison still has its limitations. Although several models have been proposed to describe the linear rheological behavior of polymer networks, many of these contain idealizations that may not apply to a polymer solution from practice, like guar gum. Therefore, a comprehensive mapping between one of these models and our observations is not to be expected. In the following, we will investigate which of the existing models gives predictions that bear the closest resemblance to our observations.

The appearance of two storage modulus plateau zones indicates the occurrence of two distinct mechanisms for relaxing the stresses imposed via the oscillatory deformation. In a polymer network, stresses are induced via distortions of the chain distribution function. This can involve both the orientation and the length of chains or chain strands. Since our polymer solutions are all above c^*, and since physical associations between polymer chains can be expected, two mechanisms that should be considered at first are the breakup of bonds and diffusion of chain (strands) out of confining tubes (reptation). To take into account the possibility that the two types of relaxation are independent, we will first compare our measurements with models that predict only one relaxation. Thereafter, coupled relaxations will be considered.

4.1. Reptation Model. For fluids containing entanglements, one of the possible relaxation mechanisms to consider is the diffusion of chains along their contours. This process, called reptation has been modeled by Doi and Edwards.[7] In this model, the chains do not form physical bonds with each other, but there are topological constraints which restrict the transversal motion of chains.

The reptation model predicts one storage modulus plateau and a relaxation spectrum spanning approximately 1 decade. Comparing the predictions of the Doi–Edwards model with our experimental observations for the monodisperse system (shown in Figure 5), it is clear that the model is not able to describe the experimental high-frequency relaxations, which span almost 3 decades in frequency.

Other discrepancies become evident from the comparison presented in Table 5. According to the reptation model, the scaling of $\tau_{G'=G''}$ and the zero shear viscosity (with the polymer concentration and the molecular weight) would correspond to much weaker powers than

Table 5. Predicted Scaling Behavior, According to Reptation[a]

reptation scaling	M_w	c
η_0	3 (5.8)	3.75 (4.5)
$G_{G'=G''}$	0 (0)	2.25 (1.8)
$\tau_{G'=G''}$	3 (6.7)	1.5 (2.7)

[a] Numbers in parentheses indicate experimental values.

observed in the experiments. An exception is the *scaling* of the magnitude of the moduli, but considering the *magnitude* of the storage modulus G_0, again a discrepancy is found. According to the model, the number of steps in a primitive chain (L/a) (the number of tube segments) follows from G' via

$$G_0 = N_c \frac{L}{a} kT \tag{4}$$

with N_c the number of chains per unit volume. Here a is a parameter which is on the order of the mesh size of the network which defines the tube. When we take for example the storage modulus of 20 Pa for the 0.5% (w/w) guar HM solution, we obtain a number of steps in the primitive chain equal to 2. Obviously the concept of a confining tube, which forms a key element in the reptation model can only hold for $(L/a) \gg 1$.

Considering the various discrepancies, it can only be concluded that our observations for the linear rheological behavior cannot be interpreted with "simple" reptation (i.e., as described by Doi and Edwards[7]), not even when restricting to a certain part of the frequency domain (0.03−100 Hz).

4.2. Associative Polymer Solution Model. Recently Bromberg[3] and English et al.[11,12] reported experimental studies on the rheological behavior of associative polymers. Some observations with a striking similarity to ours were made in these investigations. Bromberg[3] found an unusually strong temperature dependence for the storage modulus, comparable to the temperature dependence we found for $G'(\omega)$ at low frequencies. English et al.[11] found storage moduli that were not proportional to ω^2 in the low frequency regime, where this limiting behavior is usually observed. Instead they observed a slope of 0.7 in a log−log plot. Also this is in qualitative accordance with our observations. Already in the beginning of section 4, we have argued that chain associations are to be expected on molecular grounds. These notions make it interesting and appropriate, to consider predictions of rheological models developed for associative polymers.

In 1998, Semenov and Rubinstein presented a comprehensive modeling for associative polymer solutions, including predictions for the linear viscoelastic behavior.[30−32] Polymers with associative sites (stickers) along the chain will form clusters in solution. Above a certain threshold concentration c_g, the clusters will connect to a space-filling network. We will discuss only the two possible regimes above this threshold concentration, since only there is a storage modulus plateau zone predicted, which can be compared to our experimental $G'(\omega)$ data above 10 Hz.

Just above the gel concentration c_g, the network consists of large clusters which are singularly connected with each other via so-called "critical bonds". When such a bond is broken, a cluster is released from the network and will quickly relax its stress in a Rouse-like manner. The relaxation time is then determined by the time it takes to break up the critical bonds (see Figure 12 for an illustration). At higher polymer concentrations, a strong transient network will be formed, in which each chain is multiply connected to other chains in the network. Here critical bonds do not exist anymore and the relaxation process has become the multiple breakup of bonds before chains can undergo Rouse relaxation. To investigate the applicability of the Semenov and Rubinstein (S&R) model we consider both regimes in the following.

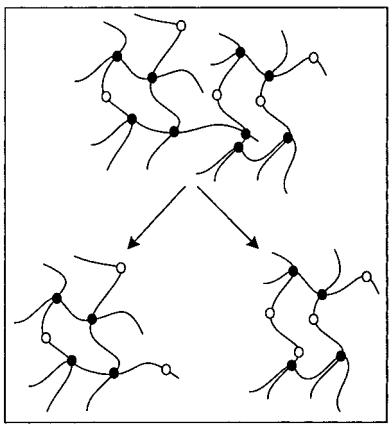

Figure 12. Cartoon of the breakup of a critical bond.

4.2.1. Weak Network Regime. To make a comparison with the model, we have assumed that, for all molecular weights and concentrations, our samples were just above the gelation threshold. The number of stickers per chain is expected to increase proportionally with the molecular weight. According to S&R,[32] c_g is then proportional to the chain length to the power $(1 - 3\nu)/(1 + z)$, with $\nu = 0.59$ and z depending on the solvent quality. Assuming good solvent conditions for the chain without stickers, $z = 0.225$. The scaling of the storage modulus plateau G_0 can then (using eq 3.16 of S&R[32]) be expressed as

$$G_0 \sim \tilde{c}\tilde{M}^{-1}(\tilde{c}\tilde{M}^{0.63} - 1)^3 \tag{5}$$

with $\tilde{c} \equiv c/c_g^0$, $\tilde{M} \equiv M/M_0$ and c_g^0 the value of c_g at reference molar mass M_0. According to eq 5, the dependence of G_0 on c or M will not show linearity in a log−log plot. However, in the limiting case of $\tilde{c}\tilde{M}^{0.63} \gg 1$, the local slopes will be minimal, being 4 for the concentration dependence and 0.89 for the molar mass. For smaller $\tilde{c}\tilde{M}^{0.63}$, the local slopes will be larger. Similar arguments apply to the scalings of $\tau_{G'=G''}$ and the low shear viscosity η_0. The prediction for the relaxation time, corresponding to the breakup of "critical bonds" is given by

$$\tau \sim \tilde{c}\tilde{M}^{0.63} - 1 \tag{6}$$

and the prediction for the zero shear viscosity is

$$\eta_0 \sim \frac{1}{\tilde{M}^{1.63}}(\tilde{c}\tilde{M}^{0.63} - 1)^4 \tag{7}$$

The lower bounds for the power law coefficients are listed in Table 6. Except for the concentration dependence of the zero shear viscosity, the predicted power laws are not observed in our measurements, and in particular, the minimal predicted powers for $G_0(M_w)$ and $G_0(c)$ are higher than the observed powers. Also, the shapes of the predicted scaling curves (which are on a

Table 6. Predicted Minimal Scaling Behavior for Associative Polymer Solutions without Entanglements[a]

associative polymer scaling	M_w	c
η_0	≥0.89 (5.8)	≥4 (4.5)
$G_{G'=G''}$	≥0.89 (0)	≥4 (1.8)
$\tau_{G'=G''}$	≥0.63 (6.7)	≥1 (2.7)

[a] Numbers in parentheses indicate experimental values. See text for further details.

log−log scale steadily increasing concave functions with asymptotic power law behavior) do not agree with the observed shapes in Figures 8, 9, and 11 which are either linear or slightly convex functions.

Therefore, we can conclude that the model of Semenov and Rubinstein for the weak network (critical bonds) regime does not correspond well to our experimental data.

4.2.2. Strong Network Regime. For a strong network, the chains would have to be multiply connected to other chains and the absolute magnitude of the observed storage modulus plateaus should indicate so. From the measured values, the mean number of connections per chain can be accounted, comparable to the calculation in section 4.1 for the number of entanglements per chain. This leads to a the mean number of connections per chain of 2 in the case of a 0.5% (w/w) guar HM solution, indicating that for the lower experimental polymer concentrations, the chains are on the edge of being singly or multiply connected.

According to the model of Semenov and Rubinstein, the relaxation time dependence changes for a strong network into

$$\tau \sim \tilde{c}^{3.2}\tilde{M}^2 \tag{8}$$

Our observed molecular weight dependence of the relaxation times (belonging to the high storage modulus plateau) differs strongly from this prediction. Hence also this regime of the S&R model bears no resemblance to our observations.

4.3. Hindered Reptation. It was already mentioned in the Introduction that specific polymer−polymer interactions as well as reptation might play a role in the observed rheological behavior of guar gum. Therefore, we will now discuss the model of hindered reptation[20] (by Leibler, Rubinstein, and Colby), denoted in the following as LRC. In this model each polymer chain is supposed to contain many association sites. The chains are also entangled with each other and therefore diffusion is only possible along the chain.

To understand the relaxation processes that take place, let us consider the step−strain experiment in which polymer chains will be stretched and placed in preferred orientations. Since the chains are connected via physical bonds to the rest of the system, the whole chains will not be able to return to their equilibrium length at once. Only the *loose chain ends* can perform such a (virtually instantaneous) Rouse relaxation. The parts of the chains that belong to the network have to remain stretched until the bonds are thermally broken. These strands are only able to reach their equilibrium length after all bonds have been broken at least once. After stress has been released via this mode, there will still be residual stress, since the preferred orientations have remained. To restore the equilibrium orientation distribution, the chains have to diffuse reptation-like out of their tubes (which represent their topological constraints). This diffusion process can only take place for chainstrands that are not directly connected via bonds to the rest of the system. Since the bonds break and form continually, chain strands are only temporarily not connected to the system. In this fashion, the presence of stickers acts to slow the diffusion process. It is via this so-called hindered reptation, that the chains will acquire random orientations and release the remaining stress.

The relaxation time belonging to Rouse relaxation of the *network strands* is in the model set equal to the breakup time of a physical bond: in other words the breakup event is modeled as a trigger for these Rouse relaxations. Assuming thermal breakup as a random event, characterized only by a temperature-dependent probability, the temperature dependence of the relaxation time is modeled with an Arrhenius equation. The equalization also implies that the relaxation time is predicted to be independent of the molecular weight. With respect to the dependence on concentration, no predictions are made in the LRC model.

The second and longest relaxation time is determined by both the reptation and the breakup time scales. In the case that the relaxation times of thermal breakup and of the hindered reptation are well separated, the LRC model predicts two storage modulus plateaus as shown in Figure 13. The magnitude of the low frequency plateau must obviously be identical to the one predicted by the Doi−Edwards model, and the magnitude should scale with the polymer concentration to a power of 2.25.

When we confront these predictions with our experimental data, we see in both cases two storage modulus plateau zones. The observation that the relaxation time, corresponding to the high frequency plateau, shows an Arrhenius-like temperature dependence is explainable with the breakup of stickers involving a certain activation energy. Also this would be in accordance with the LRC model. An observation not covered by the LRC model is that the relaxation time associated with the thermal breakup, was in our experiments found to depend strongly on molecular weight.

A more serious difference between the model and the experiments becomes evident when the magnitude of the low frequency G' plateau is considered. As in the discussion of the Doi−Edwards model, again eq 4 can be used to estimate the number of tube segments ((L/a)). Applying this method now to the *low frequency* G' plateau, we find for the 0.5% (w/w) guar HM solution a number of only 0.05 which means that the network mesh size is large compared to the tube length. Therefore, we cannot justify the attribution of the low frequency relaxation to reptation. In addition we would like to point out that it is not only the *magnitude* of the low frequency G' plateau that fits poorly. Also, its concentration dependence is much weaker than the predicted scaling with a power of 2.25. This makes the reptation of *single chains* an unlikely cause for the storage modulus plateau at low frequencies.

4.4. Two Types of Associations. Another possible reason for the occurrence of two distinct relaxations could be a variability in the stickers present on the guar chains. It has been suggested that a minimum number of six free backbone units in a row is needed to form a stable bond.[15] Following this reasoning, it is conceivable that stronger bonding is achieved for an increased number of subsequent bare backbone units. In the simplest case, this situation could be represented by a two-sticker model. Therefore, we will now discuss a

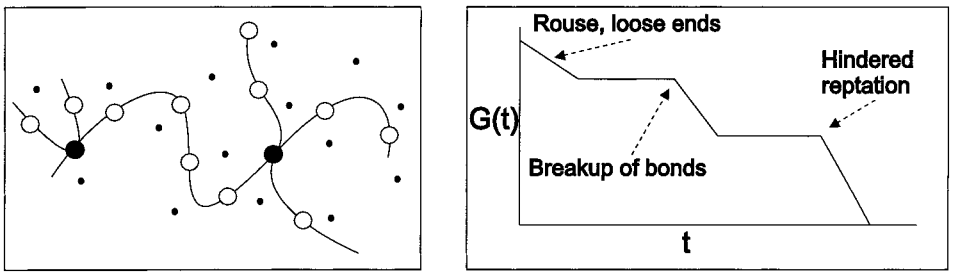

Figure 13. Snapshot of a polymer showing hindered reptation (left) and the corresponding predictions for the relaxation behavior (right). The dots are the surrounding polymers.

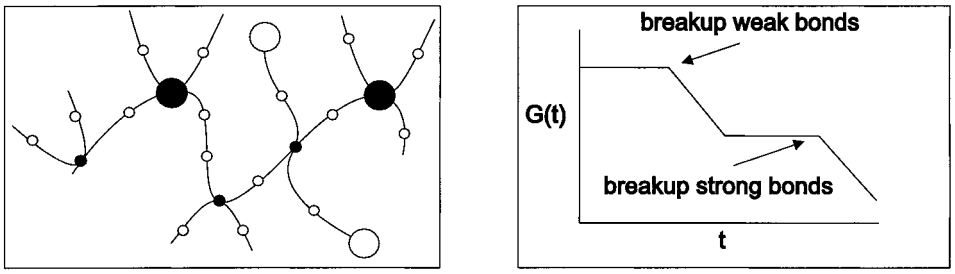

Figure 14. Cartoon of a transient network with strong and weak physical bonds (left), and the corresponding predictions for the relaxation behavior (right).

recently developed model in which two types of physical bonds cause two different relaxation possibilities.[17,34]

In these models, it is assumed that the polymer chains contain regularly spaced association sites (stickers), which are available for physical bonding. In solution a transient network is formed, of which the dynamics is governed by the breakup and forming rates of the bonds. Equality between these rates (detailed balance) defines a steady state. All stickers are considered to be present in one and the same network (as illustrated in Figure 14).

An important ingredient of the model (and also an improvement compared to earlier models) is that the connectivity of the chains is taken into account. All network strands that are enclosed between two bonded stickers are modeled to carry stress. Here the bonded stickers may be provided by *any* of the association sites located on the same chain. Chain strands that become part of loose ends, are supposed to release their stress instantaneously. Chain parts *not* constituting loose ends are supposed to carry stress due to their confinement in virtual tubes. Here the tubes represent the topological constraints imposed by the other chains in the network. Because of the introduction of these concepts, the predicted relaxation spectrum shows a dependency on the number of stickers per chain N_{st} (which has the molecular weight as its experimental counterpart). Both $\tau_{G'=G''}$ and the broadness of the time spectrum are predicted to increase with N_{st}.

It is now a simple matter to qualitatively explain the predicted relaxation behavior of this model. In a step−strain experiment, all chain strands that are enclosed between two bonded stickers will be stretched and will take preferred orientations. Subsequently, stress will be released via the breakup of bonds as explained above. First, stress will be released on the shortest time scale of breaking the weak bonds. What remains after this relaxation is the stress of the network held together by the strong bonds. The breakup time of these bonds is longer, and in case the two breakup times are very different, the relaxation behavior will resemble that of Figure 14.

Two important model quantities that lend themselves to a comparison with experimental results are the breakup time(s) and the number density of bonds. The former quantity can be identified as proportional to the relaxation time whereas the latter is proportional to the storage modulus plateau. To calculate them, the breakup and forming rates (h and g) need to be specified. We would like to point out here that the dependencies of these rates on experimental variables (like the temperature and concentration) are not specified by the model itself, and hence need to be separately introduced.

A concentration dependence for h and g can be incorporated by assuming that breakup is an independent process and that the formation of a bond involves a random encounter of two stickers. In that case $h \sim n_{\bullet\bullet}$ and $g \sim n_o^2$ with n_o and $n_{\bullet\bullet}$ the number densities of open stickers and closed sticker-pairs, respectively. The steady state is then characterized by a chemical equilibrium constant, i.e.

$$\frac{n_{\bullet\bullet}}{n_o^2} = \frac{\frac{1}{2}Nx}{N^2(1-x)^2} = K \qquad (9)$$

where x is the fraction of bonded stickers. N is the total number density of association sites (irrespective of whether they are bonded or not) and is proportional to the polymer concentration. Recalling that the relaxation strength G' is proportional to the number density of bonds Nx, it is easily verified that $G' \sim N^2$ for small K ($x \ll 1$) whereas $G' \sim N$ for large K ($x \approx 1$).

The temperature dependence of h and g can be modeled with Arrhenius equations (like eq 2). The rates are then expressed in their respective activation energies (E_b for breakup, E_f for forming) and the temperature. Combining this proposed temperature dependence with the proposed concentration dependence, the equilibrium constant K would scale as

$$K \sim e^{(E_b - E_f)/kT} \qquad (10)$$

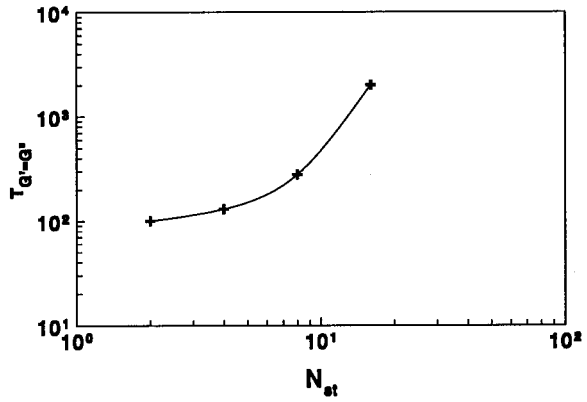

Figure 15. Typical result of the dependence of the mean relaxation time on the number of stickers per chain, according to the model of Jongschaap et al. in the case that $K = 1$.

The dependence of the relaxation time upon the molecular weight (in terms of the model: N_{st}) cannot be chosen but is defined by the model. This dependence is qualitatively an increasing convex function. Figure 15 shows a typical result of this dependence. It can be seen that the local slope depends strongly on the number of stickers per chain.

Comparing these predictions to our experimental data, we see in both cases two storage modulus plateau zones together with the broad relaxation spectrum. Also the dependence of $\tau_{G'=G''}$ upon the number of stickers per chain (Figure 15), matches qualitatively with its experimental counterpart (in Figure 9b): increasing and slightly convex. Assuming that six free backbone units are needed to form a stable weak bond[15] and that the galactose units are placed randomly on the backbone chain, the number of stickers on the chain is of order 10, but is difficult to pinpoint precisely. The local scaling power of roughly 3.0 for 10 stickers per chain is obviously low compared to the observed 6.7, but as mentioned above, the slope depends strongly on the number of stickers, which could only be roughly estimated.

The found scaling power with concentration of 1.8 for the experimental high frequency G' plateau lies in predicted range and is close to 2.0 as predicted from eq 9: $G' \sim N^2$ for $x \ll 1$.

The scaling of the low frequency G' plateau with concentration and temperature is less satisfactorily described by the model supplemented with the aforementioned description for chemical equilibrium. The weak concentration dependence as evidenced by Table 4 lies below the lower limit predicted by eq 9, i.e. $G' \sim N$ for $x \approx 1$. To explain the strong temperature dependence of the low frequency G' with eqs 9 and 10, it would be required that $E_b^{strong} > E_f^{strong}$; in other words, the bonded state should have a higher energy than the free state. This is qualitatively different for the weak bonds.

Perhaps a more plausible assumption would be, to consider the weak and strong bonds to have a different nature. For example the weak bonds may be hydrogen bridges whereas the strong bonds could be of a hydrophobic nature. Hydrophobic bonds cannot be characterized by an activation energy that is more or less independent of temperature, but instead they may a show a strongly increased tendency to bonding when the temperature is raised.[16]

Summarizing, the two-sticker model of stickers is capable of successfully describing several observations, like the two storage modulus plateau zones and the temperature dependence. The flexibility of the model with respect to the choice for the creation and annihilation rates makes it both versatile and more difficult to corroborate or falsify. The concentration dependence of the storage modulus plateau at low frequencies remains difficult to understand.

5. Discussion

In this paper, we presented the linear rheological behavior of guar gum solutions. Comparing our experimental results to earlier work, no discrepancies are found. However since we investigated the moduli down to 10^{-4} Hz, we were able to observe the second storage modulus plateau zone at low frequencies. The extensive mapping of the concentration and molecular weight dependence allowed us to compare the experimental results with microrheological models. In this section, two subjects that arise from this comparison are discussed. First we discuss some (not yet worked out) model concepts that may lead to comparable predictions. Second, we make some remarks about guar gum as a model system and comment on the need to obtain additional information about the mesoscopic structure.

5.1. Other Model Concepts. Comparison our experimental data on guar gum with different microrheological models has shown that existing models can predict qualitatively only parts of the observed behavior. This was not unexpected, since the models are based upon idealizations that are needed for simplicity which do not apply to guar gum solutions. However, from this comparison it became clear that not even a part of the frequency behavior is described by the reptation model and that physical bonds are needed most likely for explaining the complex overall behavior.

From the predictions of the different associative polymer models we can conclude that the picture of having two types of stickers with a clearly different bonding behavior (different energies needed for breakup and forming) leads to the closest match with the experiments. Sticking to the concept of having two different relaxation mechanisms, determined by different physical bonds, we can also think of other (not yet developed) model ideas. An important difference between these ideas and the model presented in section 4.4 is that only a few strong bonds (and no weak bonds) are assumed to be present per chain.

Assuming a few strong bonds would lead to large polymer structures, more or less comparable to star polymers. For star polymers also two storage modulus plateau zones have been reported by Pakula et al.,[25] Vlassopoulos et al.,[33] and Kapnistos et al.[18] They compared their experimental results to predictions from Milner and McLeish[22] for starlike polymers and found an extra storage modulus plateau at low frequencies. To explain this, a mesoscopic structuring of the star polymers was proposed, similar to that of dense colloidal particle systems. The central parts of stars with a high number of arms are then considered as cores occupying a volume excluded for elements of neighboring stars. Because of this, the centers of mass of these stars show distinct positional correlations in the sense of a configurational distribution function. The free energy stored in this configuration then causes the storage modulus plateau at low frequencies.

When we assume that, in our experimental system, polymer chains form a few strong physical bonds with

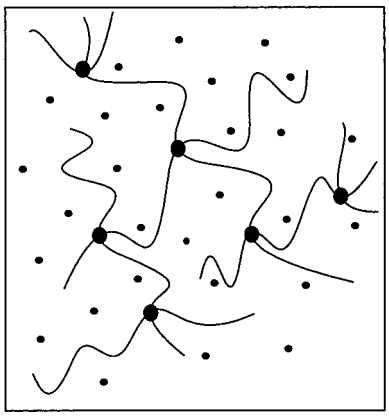

Figure 16. Large starlike reptating structures, formed by physical bonds. The dots present the surrounding polymer chains.

a very long lifetime, these bonds will cause the formation of large structures, similar to polymer stars but with nonlinear and nonmonodisperse polymer arms. These structures will also show slow structural rearrangements on a long time scale, caused either by the breakup of strong bonds or via a diffusive relaxation of the mass centers of these "stars". On a short time scale, the classical arm retraction mechanism will be observed (reptation of stars) which causes the storage modulus plateau at high frequencies. Figure 16 shows an example of such a starlike polymer structure.

This model idea would predict two storage modulus plateau zones and a very broad relaxation spectrum (belonging to the arm retraction mechanism), since the distribution of starlike arms will clearly be polydisperse. When we assume that the via strong physical bonds formed stars do have only a few arms (4−6) we can predict a strong molecular weight dependence for the relaxation time and the zero shear viscosity since they already show an exponential behavior upon the molecular weight for "normal" starlike polymers.[7] In fact, Lusignan et al.[21] measured in 1999 the viscosity of randomly branched polymers as a function of the molecular weight of the linear polymer chain arms. They found a scaling of 6.0 where we found a scaling of 5.8 ± 0.2. In the case that the long time scale process is caused by the breakup of strong (hydrophobic) bonds, the found temperature dependence for the storage modulus plateaus at low frequencies can be predicted qualitatively (see section 4.4).

So, although the two-sticker model (discussed in section 4.4) predicts qualitatively many of the observed phenomena, other model concepts which predict qualitatively the same behavior are also conceivable. At present, we cannot make a sharp distinction between these. A very suitable experiment for getting a sharper focus would be to remove part of the galactose side groups by means of enzymatic modification (and study the rheological consequences). In case the relaxation between 0.1 and 10 Hz would involve the breakup of hydrogen bridges, modest changes in $G'(\omega)$ are expected. But in the case of starlike reptation of loose ends, the length distribution of these ends may change significantly, giving rise to more noticeable changes in $G'(\omega)$. These experiments will be done in a future study.

5.2. The Mesoscopic Structure. Although the frequency spectrum between 0.1 and 10 Hz is easily characterized regarding the dependencies on experimental variables (time−temperature and time−concentration superposition), the shape of the spectrum and the relaxation strengths can be only qualitatively mapped with existing microrheological models. The behavior at lower frequencies is more difficult to understand and describe, since here the relaxation times are difficult to probe.

Our primary goal was, however, to understand and describe the linear rheological behavior of guar gum. Our systematic investigation of the dependencies on T, c, and M have made it possible to rule out classical relaxation mechanisms. However, pinpointing alternative mechanisms that are in agreement with all observations is difficult. The identification of associative sites as the mechanism responsible for stress relaxation at low frequencies was made on the basis of exclusion of other possibilities, combined with chemical information. And it is the models with the lowest specificity that best survive the comparison with experimental data. On one hand, this reflects that the state of art in modeling has not proceeded far enough for covering the complex and diverse behavior of associative polymers. On the other hand, it underlines the need for information in addition to rheological data.

Additional experiments aimed at understanding the chemistry or elucidating the structure may further guide interpretation and modeling. It is however difficult to find suitable techniques for characterizing the guar. However, scattering experiments like SANS may help to obtain more information about the internal structure and to understand the mesoscopic structure.

6. Conclusions

From our extensive investigation of the rheological behavior we can conclude that at high frequencies guar gum (>100 Hz) solutions show Rouse behavior. At lower frequencies, guar gum shows two storage modulus plateau zones and a very broad relaxation spectrum (at the high storage modulus plateau) which is not caused by polydispersity.

Guar gum shows very strong scaling behavior with molecular weight and polymer concentration as can be seen in Table 3. Recent investigations demonstrate that associative polymer systems generally show strong scaling behavior, comparable to our observations. The exception from these strong scalings is the scaling of the storage modulus plateau zones. The plateau at high frequencies scales as predicted by reptation. Still, the scaling lies also in the range of what can be expected by assuming physical bonds. The plateau at low frequencies however scales very weak with the concentration and the molecular weight and it is not clear what causes this weak dependence.

Comparison with different microrheological models showed that two or more relaxation mechanisms are needed for explaining this complex behavior. The classical reptation model cannot even predict a part of the observed frequency behavior, and at least one type of physical bonds is needed for obtaining qualitatively correct predictions. However it was not possible to discriminate between the model ideas of two types of associations (section 4.4) and starlike structures caused by strong physical bonds (section 5). For a better understanding of the relaxation mechanisms that cause the rheological behavior of guar gum solutions, more information would have to be obtained about the in situ mesoscopic structure. This could make a more specific modeling both feasible and appropriate.

Acknowledgment. We thank Rob Vreeker and Wim Agterof (Unilever Research Laboratories, Vlaardingen) for fruitful discussions. Rainer Hoffman (Unilever Research Laboratories, Colworth) is kindly acknowledged for the characterizations with GPC. We thank Roel Vromen for performing part of the rheological experiments. This work is part of the research program of the "Stichting voor Fundamenteel Onderzoek der Materie (FOM)" and is financially supported by Unilever.

List of Symbols

a = parameter of the reptation model which is of order of the mesh size of the network (m)
a_T = frequency multiplication factor
c = polymer concentration (g/L)
c^* = critical concentration (g/L)
c_g = gel concentration (g/L)
c_g^0 = value of c_g at reference molar mass M_o (g/L)
$\tilde{c} = c/c_g^0$
E_{ap} = apparent activation energy (kT)
E_b = activation energy for breakup (kT)
E_f = activation energy for forming (kT)
f = frequency (Hz)
G' = storage modulus (Pa)
G'' = loss modulus (Pa)
G_0 = storage modulus plateau (Pa)
g = forming rate (1/s)
h = breakup rate (1/s)
h_c = Huggins coefficient
k = Boltzmann constant
k_{MH} = Mark−Houwink constant (L/g)
K = chemical equilibrium constant
L = contour length of the primitive chain (m)
M_w = weight-average molecular weight (Da)
M_0 = reference molar mass (Da)
$\tilde{M} = M/M_0$
$n_{••}$ = number density of closed sticker pairs (m^{-3})
n_o = number density of open stickers (m^{-3})
N = number density of association sites (m^{-3})
N_{st} = number of stickers per chain
N_c = numer of chains per unit volume (m^{-3})
T = temperature (K)
T_{ref} = reference temperature (K)
x = fraction of bonded stickers
$z = 0.225$
α = Mark−Houwink constant
$\dot{\gamma}$ = shear rate (1/s)
η = steady shear viscosity (Pa s)
η^* = complex viscosity (Pa s)
η' = dynamic viscosity (Pa s)
η_0 = zero shear viscosity (Pa s)
η_s = solvent viscosity (Pa s)
$[\eta]$ = intrinsic viscosity (L/g)
η_{red} = reduced viscosity (L/g)
$\nu = 0.59$
τ = relaxation time (s)
$\tau_{G'=G''}$ = characteristic relaxation time (s)
ω = angular frequency (rad/s)

References and Notes

(1) de Belder, A. N.; Granath, K. *Carbohydr. Res.* **1973**, *30*, 375−378.
(2) Blom, C.; Mellema, J. *Rheol. Acta* **1984**, *23*, 98−105.
(3) Bromberg, L. *Macromolecules* **1998**, *31*, 6148−6156.
(4) McCleary, B. V.; Nurthen, E.; Taravel, F. R.; Joseleau, J. P. *Carbohydr. Res.* **1983**, *118*, 91−109.
(5) Cox, W. P.; Merz, E. H. *J. Polym. Sci.* **1958**, *28*, 619−622.
(6) Dea, C. M.; Morrison, A. *Adv. Carbohydr. Chem. Biochem.* **1975**, *31*, 241−312.
(7) Doi, M.; Edwards, S. F. *The theory of polymer dynamics*; Clarendon: Oxford, England, 1986.
(8) Doublier, J. L.; Launay, B. *Proc. Int. Congr. Rheol., Gothenburg, 7th* **1976**, 532−533.
(9) Doublier, J. L.; Launay, B. J. *Text. Stud.* **1981**, *12*, 151−172.
(10) Van den Ende, D.; Blom, C.; Mellema, J. *Proc. Eur. Congr. Rheol., Sevilla, 4th* **1992**, 525−527.
(11) English, R. J.; Gulati, H. S.; Jenkins, R. D.; Khan, S. A. *J. Rheol.* **1997**, *41*, 427−444.
(12) English, R. J.; Gulati, H. S.; Jenkins, R. D.; Khan, S. A. *J. Rheol.* **1999**, *43*, 1175−1194.
(13) Gidley, M. J.; Eggleston, G.; Morris, E. R. *Carbohydr. Res.* **1992**, *231*, 185−196.
(14) Goff, H. D.; Ferdinando, D.; Schorsch, C. *Food Hydrocolloids* **1999**, *13*, 353−362.
(15) Goycoolea, F. M.; Morris, E. R.; Gidley, M. J. *Carbohydr. Polym.* **1995**, *27*, 69−71.
(16) Haque, A.; Jones, A. K.; Richardson, R. K.; Morris, E. R. In *Gums and stabilisers for the food industry 7*; Philips, G. O., Willams, P. H., Wedlock, D. J., Eds.; Oxford University Press Inc., New York, 1994; pp 291−300.
(17) Jonschaap, R. J. J.; Wientjes, R. H. W.; Duits, M. H. G.; Mellema, J. Submitted for publication.
(18) Kapnistos, M.; Semenov, A. N.; Vlassopoulos, D.; Roovers, J. *J. Chem. Phys.* **1999**, *111*, 1753−1759.
(19) Lapasin, R.; Pricl, S. In *Rheology of industrial polysaccharides*; Blackie Academic & Professional: London, 1995.
(20) Leibler, L.; Rubinstein, M.; Colby, R. H. *Macromolecules* **1991**, *24*, 4701−4707.
(21) Lusignan, C. P.; Mourey, T. H.; Wilson, J. C.; Colby, R. H. *Phys. Rev. E* **1999**, *60*, 5657−5669.
(22) Milner, S. T.; Mcleish, T. C. B. *Macromolecules* **1997**, *30*, 2159−2166.
(23) Morris, E. R.; Cutler, A. N.; Ross-Murphy, S. B.; Rees, D. A. *Carbohydr. Polym.* **1981**, **1**, 5−21.
(24) Oosterbroek, M.; Waterman, H. A.; Wiseall, S. S.; Altena, E. G.; Mellema, J.; Kip, G. A. M. *Rheol. Acta* **1980**, *19*, 497−506.
(25) Pakula, T.; Vlassopoulos, D.; Fytas, G.; Roovers, J. *Macromolecules* **1998**, *31*, 8931−8940.
(26) Richardson, R. K.; Ross-Murphy, S. B. *Int. J. Biol. Macromol.* **1987**, *9*, 250−256.
(27) Robinson, G.; Ross-Murphy, S. B.; Morris, E. R. *Carbohydr. Res.* **1982**, *107*, 17−32.
(28) Ross-Murphy, S. B. *J. Rheol.* **1995**, *39*, 1451−1463.
(29) Rouse, P. E. *J. Chem. Phys.* **1953**, *21*, 1272−1280.
(30) Rubinstein, M.; Dobrynin, A. V. *Curr. Opin. Colloid Interface Sci.* **1999**, *4*, 83−87.
(31) Semenov, A. N.; Rubinstein, M. *Macromolecules* **1998**, *31*, 1373−1385.
(32) Semenov, A. N.; Rubinstein, M. *Macromolecules* **1998**, *31*, 1386-1397.
(33) Vlassopoulos, D.; Fytas, G.; Roovers, J.; Pakula, T.; Fleischer, G. *Faraday Discuss.* **1999**, *112*, 225−235.
(34) Wientjes, R. H. W.; Jongschaap, R. J. J.; Duits, M. H. G.; Mellema, J. *J. Rheol.* **1999**, *43*, 375−391.
(35) Fetters, L. J.; Graessley, W. W.; Hadjichristidis, N.; Kiss, A. D.; Pearson, D. S.; Younghouse, L. B. *Macromolecules* **1988**, *21*, 1644−1653.

MA001065P